Chemical Engineering Journal 510 (2025) 161706

Contents lists available at ScienceDirect

Chemical Engineering Journal

journal homepage: www.elsevier.com/locate/cej

Comprehensive upcycling waste siloxane liquid into H_2-enriched syngas and silicon carbide via a tandem thermochemical process

Huiyang Bi [a], Bo Wu [c], Mingyue Yan [a], Chen Sun [a,b,*], Zhongjian Li [a,b], Yang Hou [a,b], Lecheng Lei [a,b], Bin Yang [a,b,*]

[a] Key Laboratory of Biomass Chemical Engineering of Ministry of Education, College of Chemical and Biological Engineering, Zhejiang University, Hangzhou 310027, China
[b] Institute of Zhejiang University-Quzhou, No. 99 Zheda Road, Quzhou 324000, China
[c] Zhejiang Ecological Environment Group Co. Ltd., Hangzhou 310012, China

ARTICLE INFO

Keywords:
Waste siloxane
Upcycling
Syngas production
Silicon carbide
Flash Joule heating

ABSTRACT

Waste siloxane-enriched oil, an unavoidable byproduct of organosilicon industry, poses a significant risk to the environment. In this study, we propose a tandem thermochemical process for cascade utilization of waste siloxane. Through steam reforming, H_2-enriched syngas is produced, and silicon carbide (SiC) is synthesized via Flash joule heating (FJH) of the reforming residues. The maximum syngas yield of 42.2 mmol/g, with a H_2 proportion of 42.8 vol%, was achieved at 900°C under steam-feed ratio (SFR) was 2.0. As increasing SFR and temperature facilitated the broken of C–Si and C–H bond, promoting the production of CH_4 and H_2 with SiO_2-enriched residues as byproducts. High-quality 3C-SiC was then successfully synthesized by FJH of the reforming solid residues, with the superior SiC yield at a SFR exceeding 2.0. The high SiC yield is attributed to low energy consumption, minimal volatiles generation, and high reactivity of pyrolytic carbon residue. Furthermore, the derived flash SiC demonstrated promising performance as an electrode material for water evaporation-induced electricity generation device, demonstrating a stable open-circuit voltage of 502 mV and a short-circuit current of 9.80 μA. This study provides an effective solution for silicon-containing hazardous waste disposal and introduces a novel waste-derived nanomaterial for sensor development.

1. Introduction

Siloxanes are important silicon-containing derivatives that can be used as both nucleophilic and arylation reagents in organic synthesis [1,2]. They can also be used as raw materials for silicone oil and silica gel manufacturing[1,3,4]. Furthermore, modification of lithium-ion battery components (electrodes, binders, electrolytes) via siloxanes has recently emerged as a strategy to enhance ionic conductivity[5]. However, complex waste streams containing siloxanes, cyclosiloxanes, and other organic compounds are inevitably generated during synthesis and purification processes. These compounds pose significant envrionmental threats due to their bioaccumulation potential and neurotoxic effects [6,7], leading to their classification as hazardous pollutants[8].

Thermal co-processing, while widely adopted for organic liquid waste treatment[9–11], suffers from severe operational limitations. The approach generates CO_2 emission[12] alongside secondary pollutants (e.g. dioxins, furans), with silicon-containing ash limited its application. For dilute wastewater, it could be treated through physical–chemical methods including sedimentation, adsorption, and membrane separation[13,14]. Catalytic reforming presents theoretical viability for high-concentration siloxane waste liquid disposal. But the requisite use of strong reducing agents further exacerbates process costs and safety concerns, and the low conversion efficiency and poor product selectivity making it challenging to scale up catalytic reforming for waste siloxane

Abbreviations: DOMS, Diethoxydimethylsilane; DSC, Differential Scanning Calorimeter; DTG, Derivative Thermogravimetry; EDS, Energy-dispersive X-ray Spectroscopy; FFT, Fast Fourier Transform; FJH, Flash Joule Heating; HRTEM, High-Resolution Transmission Electron Microscop; ID, Inner Diameter; LHV, Lower Heating Value; PET, Polyethylene terephthalate; SFR, Steam-feed ratio; TG, Thermogravimetry; WEG, Water evaporation-induced electricity generator; XPS, X-ray Photoelectron Spectroscopy; XRD, X-ray Diffraction.

* Corresponding authors at: Key Laboratory of Biomass Chemical Engineering of Ministry of Education, College of Chemical and Biological Engineering, Zhejiang University, Hangzhou 310027, China.
E-mail addresses: sunchen1@zju.edu.cn (C. Sun), keyangb@zju.edu.cn (B. Yang).

https://doi.org/10.1016/j.cej.2025.161706
Received 20 November 2024; Received in revised form 26 February 2025; Accepted 16 March 2025
Available online 22 March 2025

disposal[15,16]. These technical shortcomings highlight the urgent need for cost-effective closed-loop valorization strategies for organic siloxane disposal.

Steam gasification emerges as a viable thermochemical pathway for converting organic hazardous waste (e.g. bio-oil and waste solvent) into syngas[17–19], circumventing the polyaromatic hydrocarbon deposition observed in conventional pyrolysis[20]. Steam's dual role as hydrogen donor and oxygen carrier facilitates selective bond cleavage, enhancing H_2 yields to 65–72 % vol while suppressing secondary tar generation[21]. In the treatment of waste printed circuit boards, steam gasification achieves nearly 2.3 times the organic matter decomposition efficiency of incineration and pyrolysis[22]. Nevertheless, compared with hydrocarbons, siloxane decomposition presents unique thermodynamic barriers due to the exceptionally high bond energies of Si–O (593 kJ/mol), Si–Si (326 kJ/mol) and Si–C (318 kJ/mol) [1], requiring external energy input for their decomposition. This process inevitably generates fine silicon oxide particles, which may adsorb residual toxic organic compounds, posing notable environmental risks.

Managing gasification residues is challenging due to their complex physical properties, diverse chemical compositions, and high disposal costs. Current treatment options, including landfilling, vitrification, and co-processing in cement kilns, demand substantial land use and fail to recover intrinsic silicon value within these residues. Due to its primarily consist of carbon, silicon and oxygen, it is viable to convert siloxane residues into silicon carbide (SiC) through carbothermic reduction and sintering. SiC is a versatile material known for its hardness, thermal stability, corrosion resistance, and wide bandgap semiconductor properties[23–27]. It is used in automotive[28], aerospace[5], and nuclear industries[29]. SiC enhance electric vehicles, its thermal stability benefits aerospace engines, and its radiation resistance is crucial for nuclear reactors. The conventional synthesis of SiC requires prolonged high-temperature conditions and utilizes toxic gases. However, constrained by inherent process limitations and unfavorable reaction kinetics, this approach suffers from slow reaction rates and excessive energy consumption. Flash Joule heating (FJH) innovatively circumvents these barriers via enabling rapid heating through capacitance discharge. This technique reaches peak temperatures of 3000 K at heating rates up to 10^5 °C/s, creating extreme reaction conditions in seconds. FJH has been successfully applied in areas such as 2D carbon material synthesis [30], nanoscale catalyst synthesis [31,32], Li-ion battery metal recycling [33,34], noble metal recovery [35] and waste glass fiber upcycling [36]. Due to its rapid processing and high temperatures, FJH presents a feasible approach to upcycle siloxane-derived residues into SiC, and sustainable SiC production from siloxane waste offers environmental benefits.

To realize near-complete valorization of waste siloxane, a tandem thermochemical process is proposed for the staged utilization of waste siloxane (Fig. 1). Initially, organic siloxane waste liquid is treated by steam gasification to produce H_2 – rich syngas and solid residues. The effects of temperature and water vapor dosage on syngas composition and carbon conversion are investigated. Subsequently, flash Joule heating is applied to upgrade the pyrolysis residue to SiC, examining how variables such as discharge voltage, material resistance, and gasification degree influences the SiC yield. Finally, the derived SiC serves as an electrode material in hydrovoltaic energy conversion. This study demonstrates an innovative pathway for upcycling waste siloxane liquids into high-value syngas and functional materials, contributing to the advancement of circular economy practices.

2. Material and methods

2.1. Materials and chemicals

The organic siloxane waste liquid was sourced from a chemical plant in Quzhou, Zhejiang Province, and its composition was analyzed using element analysis (CHNS/O mode) and ICP-OES methods, as summarized in Table 1. The carbon black was purchased from commercial channels and pre-dried at 65°C for 24 h in an oven to minimize moisture interference.

Table 1
Elemental composition of organic siloxane waste.

Element	C	H	O	Si	N	S
Content (wt %)	41.91	8.21	15.52	34.36	Not detected	Not detected

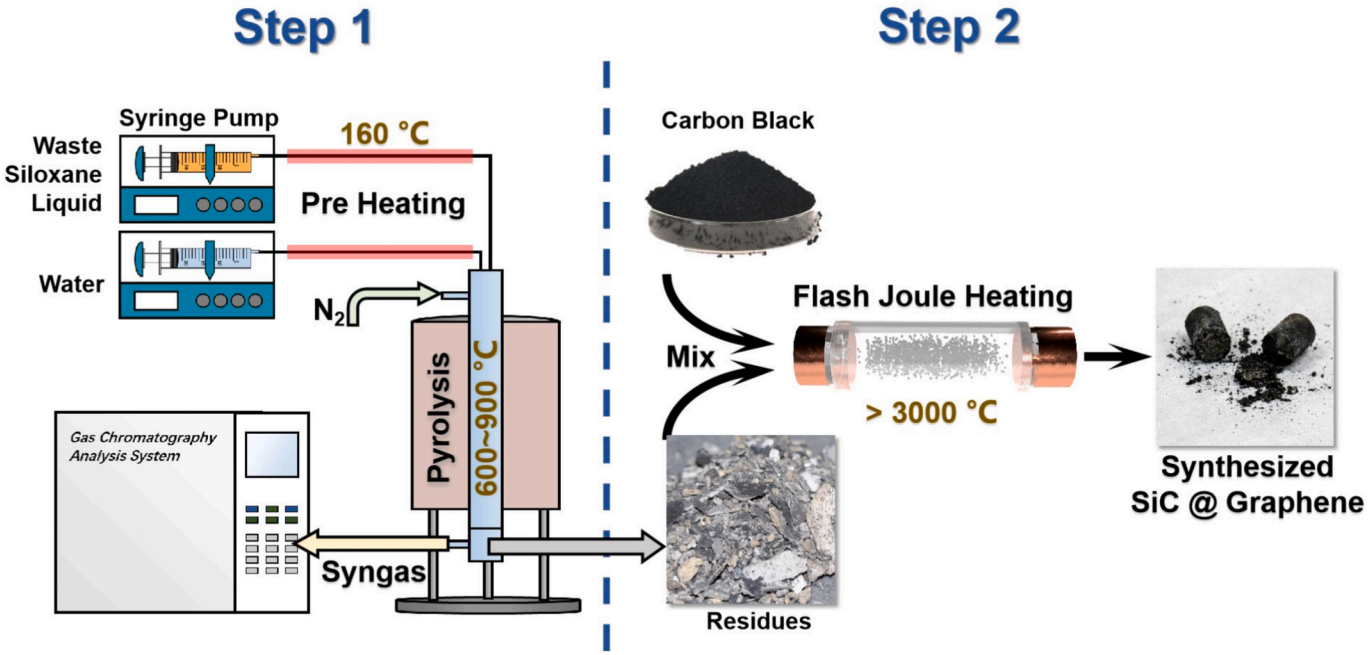

Fig. 1. Schematic of the two-step thermochemical procedures for cascade utilization of waste siloxanes. Step 1: Steam reforming of waste siloxane for syngas production in a vertical tube furnace. Step 2: Flash Joule heating of solid residues for SiC synthesis.

2.2. Steam gasification of waste siloxane

Steam gasification experiments of organic siloxane waste liquid were performed in a custom-designed continuous down-flow reactor with a vertical quartz tube (600 mm (L) × 35 mm (ID)) and a electric furnace (±1 °C precision).Prior to reaction, the reactor was purged with N_2 at 400 sccm using a mass flow controller for 30 min. The reactor was heated at a rate of 10 °C/min. The liquid feedstocks, organic siloxane waste sample and deionized water, were injected into the reactor using a syringe pump at a constant flow rate and were preheated to 160 °C for vaporization. The vaporized sample and steam were thoroughly mixed at the reactor inlet and carried by N_2 (400 sccm) for the reaction. After the reaction, the gas was filtered by a 100-mesh filter and a quartz wool-filled column to collect pyrolysis residue, and syngas was collected by using air bags (10 L) for further analysis. During the experiment, reaction temperatures were varied from 600 °C to 900 °C. The flow rate of waste siloxane was fixed at 3 mL/h, and the steam-feed ratio (SFR), expressed by mass, was set between 0 and 3.

2.3. FJH system and upcycling process

The FJH system consists of a pulse discharge device equipped with a 90 mF capacitor, a custom-made vacuum chamber, a vacuum pump, an infrared temperature detector (400–3600 °C), and a control-recording system. Pyrolysis residue was first dried in an oven at 65 °C for 12 h, and then thoroughly milled and mixed with the carbon black with a mass ratio of 20:1 to 1:1. A 100 mg portion of the mixture was placed into a quartz tube (8 mm (ID)), and it was compacted between two graphite plugs for its connection to the FJH reaction system with the whole reactor placed inside the vacuum chamber. The system was evacuated to a pressure below 1 kPa to remove air. The capacitor was charged using a direct current power supply, and then discharged through the sample inside quartz tube. The temperature, capacitor voltage, and discharge current were recorded at 1 ms interval. After the reaction, the samples were rapidly cooled to room temperature, and the residues between the graphite plugs were collected as synthetic material samples. The heat released during the FJH process was calculated as described in **Text S1**.

2.4. Fabrication of water evaporation-induced electricity generator

For fabrication of the water evaporation-induced electricity generator (WEG), SiC material was synthesized via optimized FJH treatment condition with pyrolysis residue produced at a SFR of 2.0, a material resistance of 3 Ω, and a flash voltage of 150 V. The resulting materials was dispersed in deionized water containing 0.1 wt% sodium dodecyl sulfate through 30 min ultrasonication. The stable dispersion (10 mg/mL) was then deposited on a PET non-woven fabric substrate using a simple in situ coating and drying method for WEG assembly, and the resistance of WEG was adjusted by varying the coating times. For comparison, synthetic graphene derived from carbon black under the same FJH parameters was similarly applied to a PET substrate to evaluate power generation performance at the same resistance.

2.5. Characterization

Syngas was analyzed using a Fuli GC9790 Plus gas chromatography system equipped with three detectors, allowing for both qualitative and quantitative analysis of the gas components after calibration. X-ray diffraction (XRD) was performed with a Rigaku Ultima IV system using a filtered Cu Kα radiation source. Raman spectroscopy was conducted on a HORIBA LabRAM Odyssey system with a 532 nm laser, applying 5 mW laser power, and a 50 × objection lens. X-ray photoelectron spectroscopy (XPS) measurements were performed on a Shimazu Kratos AXIS Supra + system, and the spectra were calibrated to the adventitious carbon C1s peak at 284.8 eV. High-resolution transmission electron microscopy (HRTEM) images and energy-dispersive X-ray spectroscopy (EDS) were obtained with a ThermoFisher Scientific Talos F200X system, operating at an accelerating voltage of 200 kV. Thermogravimetric analysis was performed using a Mettler TGA/DSC 3 + system from 100°C to 1200°C (10 °C /min) under N_2 atmosphere. FTIR spectroscopy was performed on a Bruker Invenio R Fourier transform infrared spectrometer. The WEG performances of open circuit voltage and short circuit current were measured with a CHI 660E electrochemical analyzer.

3. Results and Discussion

3.1. Steam gasification of waste siloxane

The gasification efficiency is significantly influenced by the reaction temperature and steam-to-feed ratio (SFR). Hereafter, the abbreviation LHV will be used to denote the lower heating value of syngas produced by per unit mass of waste siloxane liquid which was calculated by **Text S2**. The results (Fig. 2**a, 2d**, **Fig. S1**, and **Table S3-5**) indicated that temperature and SFR have a combined affect on the gasification efficiency.

To investigate the effect of steam on syngas compositions, experiments were conducted at different SFRs at 900 °C across varying SFRs (0.0–3.0, Fig. 2**a-c**). The introduction of steam demonstrated significant enhancement in gasification efficiency by promoting the formation of CO and CO_2, and it also influenced the LHV. At an SFR of 0.0, the syngas yield was low (4.69 mmol/g) with a carbon conversion rate of 11.86 % and an LHV of 2.73 kJ/g_{waste}, indicating inefficient siloxane decomposition. As the SFR increased to 2.0, the syngas yield and carbon conversion rate rose to 42.2 mmol/g_{waste} and 73.0 %, with methane reaching 12.10 mmol/g_{waste}, ethylene 3.56 mmol/g_{waste} and LHV 21.01 kJ/g_{waste}. CO and CO_2 also peaked at 6.98 mmol/g_{waste} and 1.41 mmol/g_{waste}, contributing 16.5 % and 3.3 % of the total syngas production, respectively. Beyond an SFR of 2, gasification efficiency declined. As SFR increased to 3, syngas yield dropped to 40.91 mmol/g_{waste} and carbon conversion to 65.3 %. However, H_2 yield continued to increase, riching 19.31 mmol/g_{waste}, while the LHV slightly decreased to 19.52 kJ/g_{waste}, indicating the decrease in the fuel properties of the siloxane pyrolysis syngas. The H_2-to-CO molar ratio of the syngas increased from 2.29 to 3.04 with the increase of SFR (**Table S4**), indicating its potential for Fischer-Tropsch synthesis.

In the case of diethoxydimethylsilane (DOMS), shown in **Text S3**, steam addition facilitated the hydrolysis of siloxanes, leading to the cleavage of Si–O–C bonds[37,38] and the formation of silanols and alcohols. The primary siloxane component of the waste liquid sample, hydrolysis reactions generated free ethanol[39,40], which enhanced ethylene production[41,42]. Furthermore, water vapor demonstrated inhibitory effects on carbon deposition[43,44], promoting the breakdown of multi-carbon components and the generation of non-condensable gases, thereby increasing the H_2 content. The presence of water vapor introduces the hydrolysis mechanisms for the pyrolysis of siloxanes. Therefore, the pyrolysis and gasification pathways of siloxane were shown in Table 2**.**

However, excessive amount of steam (SFR > 2) increased the oxidative atmosphere[45], leading to the formation of CO and inhibiting hydrocarbon production[46], consequently reducing syngas LHV. Therefore, an optimal SFR of 2.0 is recommended to enhance siloxane gasification efficiency, which maximizing syngas yield and carbon conversion rate.

The influence of temperature on gasification efficiency was evaluated at a fixed SFR of 2.0 (Fig. 2**d-f**). Syngas yield increased with temperature, rising from 20.82 mmol/g_{waste} at 600 °C to 42.23 mmol/g_{waste} at 900 °C. LHV underwent a gradual stabilization trend with its highest value of 21.61 kJ/g_{waste} at 800 °C, and declined by 2.31 % at 900 °C. H_2 yield exhibited the most significant increase with temperature, from 6.07 mmol/g_{waste} (600 °C, 29.1 % of the syngas) to 18.08 mmol/g_{waste} (900 °C, 42.8 %), which contributing to higher LHV, and the H_2-to-CO

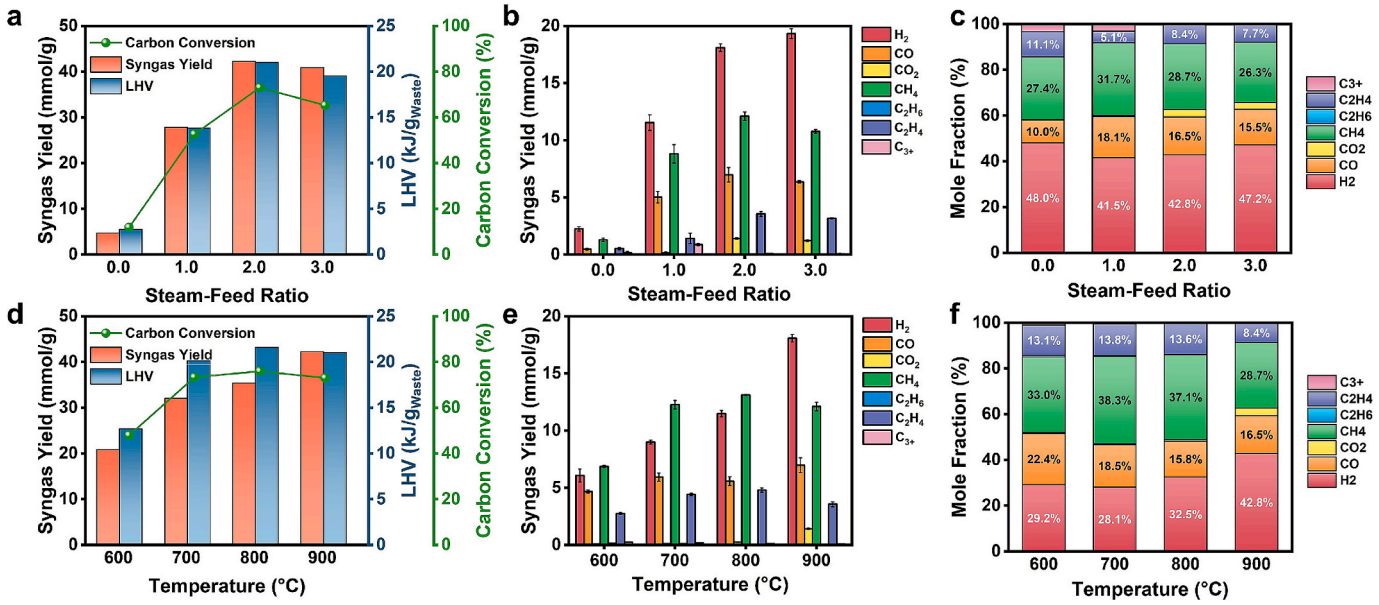

Fig. 2. Syngas generation efficiency of waste siloxane pyrolysis. a, The effect of steam-feed ratio changes from 0.0 to 3.0 on syngas production rate, LHV and carbon conversion, **b,** Syngas production by component, and **c,** composition at fixed pyrolysis temperature of 900 900 °C. **d,** The effect of pyrolysis temperature changes from 600 °C to 900 °C on syngas production rate, LHV and carbon conversion, **e,** Syngas production by component, and **f,** composition at a fixed steam-feed ratio of 2.0.

Table 2
Siloxane pyrolysis and gasification pathways.

$Siloxane + H_2O \rightarrow H_2O + SiO_2 + Gas_1 + Char_1 + Tar_1$	(1)
$Tar_1 + H_2O \rightarrow SiO_2 + Gas_2 + Char_2$	(2)
$Char_1 + Char_2 + H_2O \rightarrow Gas_3$	(3)

ratio also increased from 1.30 (600 °C) to 2.59 (900 °C). Hydrocarbon production reached its peak at 800 °C with methane and ethylene yields being 13.10 mmol/g_{waste} and 4.79 mmol/g_{waste}, while the carbon conversion also peaked at 75.9 %. The H_2-to-CO molar ratio also reached at 2.05 with a total yield of 17.05 mmol/g_{waste} (**Table S5**), which achieved the optimal ratio (2.0) for methanol synthesis and Fischer-Tropsch synthesis. At 900 °C, although the H_2 and CO flow rate peaked at 25.06 mmol/g_{waste} and showed good quality in hydrogen production, methane and ethylene yields decreased by 1.01 mmol/g_{waste} and 1.24 mmol/g_{waste}, while the yields of CO and CO_2 increased to 6.97 mmol/g_{waste} and 1.41 mmol/g_{waste}, leading to a slight decrease in LHV and carbon conversion. Similar trends were observed across other SFRs and temperatures, as shown in **Fig. S1-S3**. Thus, increasing temperature enhanced hydrogen production and syngas quality up to a point, after which excessive temperatures led to deeper oxidation, higher yields of carbon oxides, and reduced fuel quality.

3.2. *Pyrolysis residue upcycling by FJH for SiC synthesis*

After the pyrolysis of waste siloxane, silicon-enriched residues were generated, which necessitated additional treatment for comprehensive utilization. The gasification residues retrieved from the quartz tube were processed using flash Joule heat (FJH) method to synthesize silicon carbide.

Due to the low conductivity and agglomerated state of the ash, carbon black was incorporated into the residue and thoroughly milled to form a homogeneous powder mixture, aiming to reduce its resistance. During the FJH process, the mixture was packed into a quartz tube and compacted at both ends using two graphite plugs. The assembly was then integrated into an electrical circuit with a capacitor for flash heating **(**Fig. 3**a and 3b)**. Carbon black functioned as both a conductive medium and an additional carbon source in the reaction. Upon triggering the flash, the capacitor discharged at 150 V, delivering a current of ~ 210A through the sample (Fig. 3**c**), heating the sample to a peak temperature of ~ 3200 °C within milliseconds, followed by rapid cooling (~10^3 °C/s) to room temperature (Fig. 3**d**). This process was accompanied by a bright light emission (Fig. 3**b**).

After treatment, a grayish black powdery sample was obtained. The XRD patterns (Fig. 3**e**) of the sample before flash heating revealed the existence of a small amount of SiO_2 in the gasification ash. However, following the FJH process, the SiO_2 peak completely disappeared, and distinct characteristic peaks of 3C-SiC were observed at 2θ values of 35.58°, 41.38°, 59.96°, 71.76° and 75.48°, exhibiting strong intensity [47,48]. Similarly, in the Raman spectrum of the raw material, weak carbonization peaks were observed at wavenumbers of 1340 cm^{-1} and 1590 cm^{-1}. After flash heating process, the characteristic transverse optical (TO, ~790 cm^{-1}) and longitudinal optical (LO, ~970 cm^{-1}) vibration peaks of 3C-SiC appeared (Fig. 3**f**)[36]. The Si*2p* core-level analysis from XPS results (Fig. 3**g**) provided additional evidence of the transformation of the Si element during the flash treatment. It was observed that Si–O (~104.1 eV) disappeared after the flash process, while a strong and distinct Si–C peak (~100.7 eV) emerged[49,50], which indicated the cleavage of Si–O bonds and the formation of Si–C bonds.

The synthesized materials were characterized using high-resolution transmission electron microscopy (HRTEM) with an energy dispersive spectrometer (EDS). HRTEM images revealed that the sample exhibited a granular morphology (Fig. 3**h**). Element mapping via EDS (Fig. 3**i**) indicated that the particles were predominantly composed of Si and C, with minimal detectable oxygen content. Higher magnification of the sample revealed well-defined lattice fringes (Fig. 3**j**) with an interplanar spacing of 0.252 nm, corresponding to the (1 1 1) plane of 3C-SiC (Fig. 3**k**). Additionally, a fast Fourier transform (FFT) of the HRTEM image produced a reciprocal space diffraction pattern (Fig. 3**l**), which correlated with the characteristic peaks observed in the XRD analysis (Fig. 3**e**). These results further confirmed the presence of 3C-SiC in the sample after flash heating. Overall, the characterization results demonstrated the successful synthesis of SiC from gasification ash through FJH treatment. Therefore, the pathway of SiC from the pyrolysis

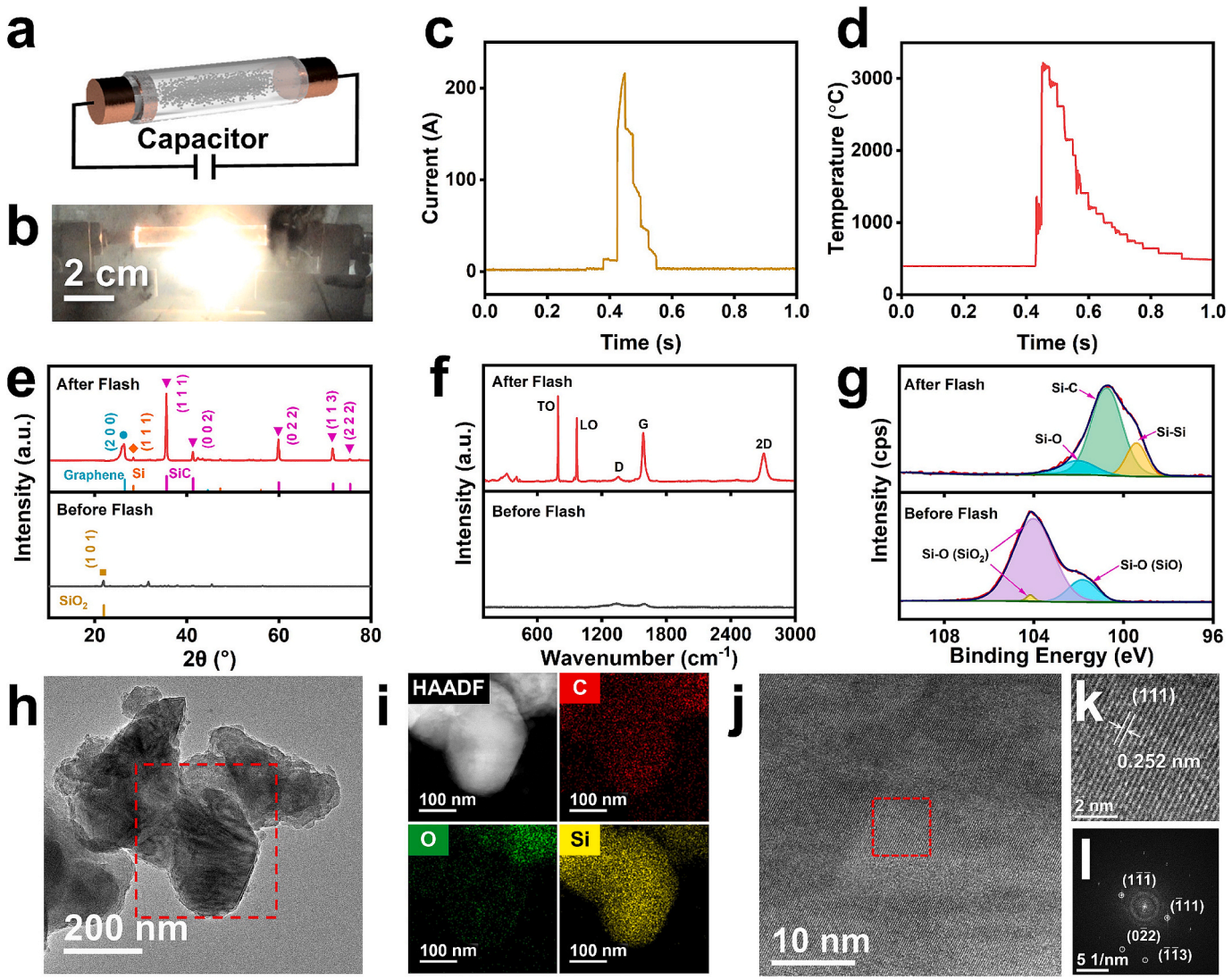

Fig. 3. Synthesis and characterization of SiC derived from siloxane derived gasification residue. a schematic of FJH reactor with samples filled into a quartz tube, **b** Picture of the sample in quartz tube during the FJH reaction. **c.** Real time current curve and **d,** temperature curve at discharge voltage of 150 V. **e,** XRD spectra, **f,** Raman spectra, and **g,** Si *2p* core-level XPS spectra of the samples before (bottom) and after (top) FJH reaction with an input voltage of 150 V. **h,** TEM image and **i,** C (red), O (green) and Si (yellow) element mapping of synthesized SiC sample. **j,** HRTEM image of synthesized SiC sample with its **k,** zoom-in image and **l,** Fast Fourier Transform image. (For interpretation of the references to color in this figure legend, the reader is referred to the web version of this article.)

residues through the FJH method can be expressed as follows[36]:

$$SiO_2 + 2C \rightarrow SiC + CO_2 \quad (4)$$

$$SiO_2 + 3C \rightarrow SiC + 2CO \quad (5)$$

Moreover, the XRD patterns exhibited graphene and weak Si characteristic peaks at 2θ of ~ 26.2° and ~ 28.4°(Fig. 3**e**), respectively. The Raman spectrum further exhibited typical features of graphene (Fig. 3**f**), including the D peak (~1350 cm^{-1}), G peak (~1585 cm^{-1}), and 2D peak (~2700 cm^{-1})[51]. Furthermore, the XPS spectrum identified the characteristic Si–Si peak at 99.3 eV (Fig. 3**g**). These results confirm the presence of graphene with low defects and trace amounts of crystalline silicon within the sample. Under the ultra-high temperature conditions of the FJH treatment, silicon-containing components (SiO_2) in the ash were carbonized and reduced to SiC facilitated by the fixed carbon in the ash and the supplemented carbon black. Excess carbon element was converted into graphene and some of the SiO_2 was converted to silicon. At high temperatures, the conversion reaction between silicon and silicon carbide can occur due to the presence of carbon and silicon dioxide. Therefore, the byproducts of the FJH process can be expressed as:

$$SiO_2 + C \rightarrow Si + CO_2 \quad (6)$$

$$SiO_2 + 2C \rightarrow Si + CO \quad (7)$$

$$SiO_2 + SiC \rightarrow 2Si + CO_2 \quad (8)$$

$$SiO_2 + 2SiC \rightarrow 3Si + 2CO(g) \quad (9)$$

$$Si + C \rightarrow SiC \quad (10)$$

$$C\,(\text{amorphous}) \rightarrow C\,(\text{graphene}) \quad (11)$$

3.3. *Factors affecting SiC synthesis*

To further improve the efficiency of synthesizing SiC materials from gasification ash, we investigated factors influencing the flash process, including the resistance of material, the applied flash voltage, and the source of gasification ash. XRD patterns of the samples were used to evaluated the crystalline phase and purity product purity of the SiC, and the intensity of the SiC characteristic peaks in the XRD patterns were

used to evaluate the variations in SiC content.

By adjusting the resistance of the material through varying amounts of carbon black (Table S6), the samples were treated with flash heating at a capacitance voltage of 150 V. As shown in Fig. 4**a**, when the initial resistance exceeded ~ 10 Ω, the characteristic peak of 3C-SiC was weak, and a SiO_2 peak at 2θ ~ 21.9° remain observable. However, when the initial resistance dropped below ~ 3 Ω, the characteristic peak of 3C-SiC increased significantly. To further quantify the SiC content, the peak area at 2θ ~ 35.6° was analyzed in conjunction with the flash heat release and the peak temperature variation with resistance at a fixed voltage (Fig. 4**b**). Results indicated that at the resistance of ~ 3 Ω, the highest flash temperature and heat release were achieved, leading to maximum SiC formation. Reducing the resistance to ~ 1 Ω by incorporating additional carbon only increased the SiC content by 2.7 %, while the flash temperature and heat release decrease. Using the thermodynamic data provided in Table S7, the Gibbs free energy changes for the SiC formation reactions (4) and (5) (Fig. S4**a**) were calculated, with their corresponding reaction temperatures determined to be approximately 2260 °C and 1480 °C, respectively. Under conditions of high electrical resistance, the instantaneous temperature can only reach a maximum of 2000 °C, rendering reaction (4) unlikely to occur. Moreover, the low carbon content associated with this reaction hinders the complete reduction of SiO_2. Conversely, lower electrical resistance not only produces a favorable thermal effect, increasing the reaction temperature to above 2400 °C, but also ensures an adequate carbon supply to sustain the reaction. As shown in Fig. 4**a**, the characteristic peak at ~ 26.2° increased with more carbon black, indicating enhanced graphene formation. Therefore, maintaining a resistance of 3 Ω is optimal for to maximizing SiC generation.

Fig. 4**c-d** illustrated the material properties and temperature characteristics under a fixed material resistance of 3 Ω when subjected to different flash voltages. At lower voltages (100 V and 110 V), the specific heating energy applied to the material was only 11.7 J/mg and 13.1 J/mg, respectively. Based on the thermodynamic data in Table S7, the Gibbs free energy changes for reactions (6)-(10) were calculated (Fig. S4**b-c**). The calculated results indicate that the threshold temperatures for forward reactions (6)-(9) are 2560 °C, 1640 °C, 2070 °C, and 2830 °C, respectively, while reaction (10) is thermodynamically favorable below 8000 °C. This indicated that elemental silicon can be predominantly produced at relatively lower reaction temperatures under sufficient carbon supply. As the applied voltage increased, the heating energy supplied to the material also rose steadily. When the voltage exceeded 150 V, the maximum flash temperatures surpassed 2500 °C, and the specific heating energy exceeded 20J/mg. At these elevated temperatures, conditions became favorable for SiC formation and elemental Si transition[36]. With a gradual increase in flash voltage, the intensity of the SiC characteristic peak correspondingly increased, consistent with the rise in specific heating energy and maximum flash temperature. This trend suggests that the higher flash voltages enhance material heating, facilitating scalable synthesis of SiC, while simultaneously suppressing the formation of the byproduct Si.

The effect of SFR on the flash process was examined, given that SFR variations during gasification influence the carbon conversion rate and, consequently, the carbon content in the gasification ash. As the SFR

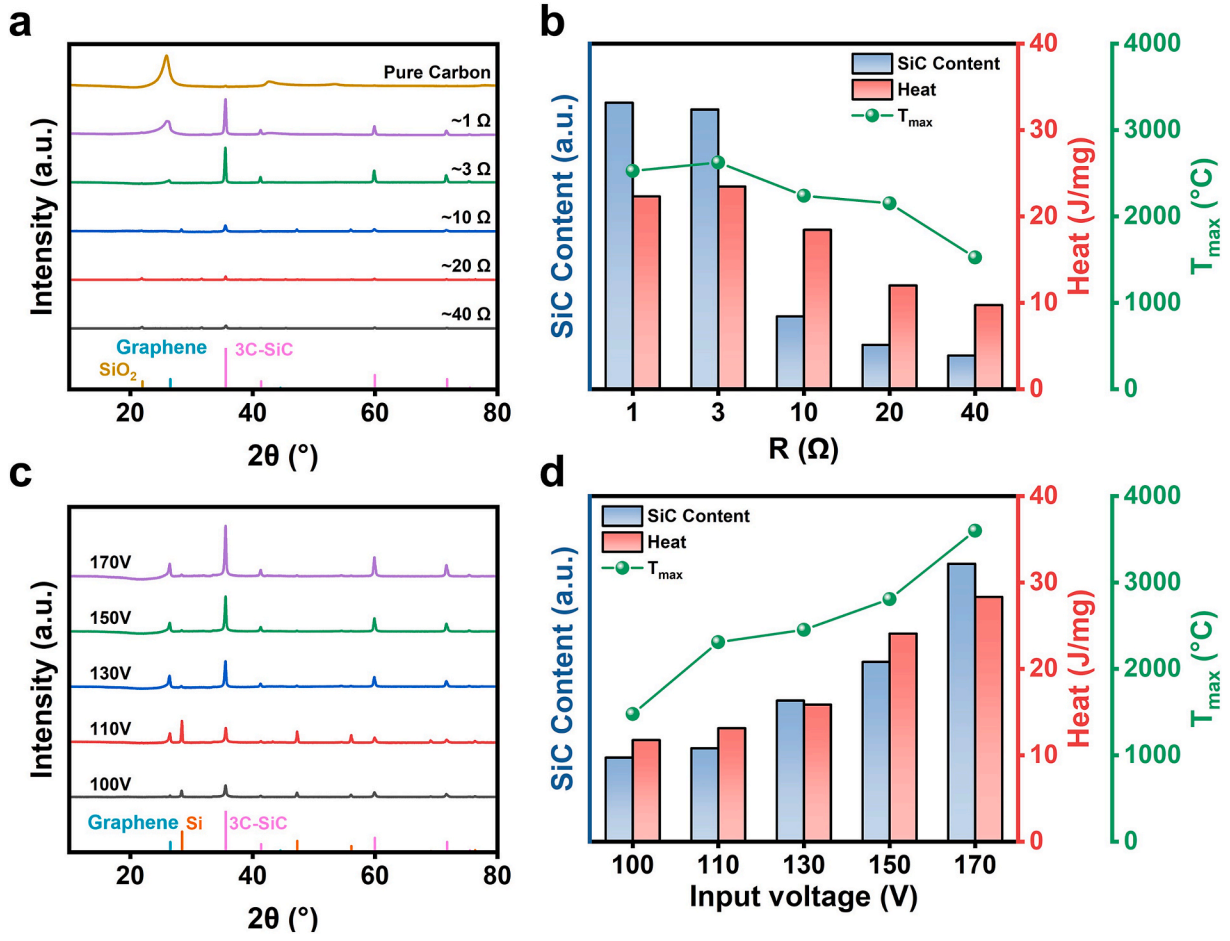

Fig. 4. Optimization of operation conditions during SiC synthesis. a-b, Effect of initial resistance and **c-d,** discharge voltage on the XRD spectra, corresponding SiC content intensity, heat released by capacitors discharge, and peak temperature. (SiC content intensity is represented by intensity of its characteristic peak at 2θ = 35.6° in the XRD spectra.).

increased from 0 to 3, the color of ash (Fig. 5**a**) transitioned from black (SFR = 0.0) through brown (SFR = 1.0) to grayish-white (SFR = 2.0 or 3.0), consistent with the carbon conversion trends in Fig. 2**a**. In this study, materials were prepared using gasification ashes collected under 900 °C pyrolysis condition with fixed FJH parameters (resistance: 3 Ω, flash voltage: 150 V). Notably, as the SFR increases, the required amount of carbon to achieve the target resistance decreased, indicating enhanced conductivity of gasification ash at higher SFR (**Table S8**). XRD patterns of the obtained materials (Fig. 5**b**) confirmed the successful synthesis of SiC. Further analysis of the exothermic properties and SiC content during the flash process (Fig. 5**c**) demonstrated that, at an SFR of 2.0, the material could be heated to over 3600 °C with a maximum heating energy of 30.6 J/mg. This condition achieved the highest SiC production efficiency. However, further increasing the SFR during the pyrolysis process slightly suppressed the SiC yield.

To investigate the differences in silicon carbide yield from the residues under varying SFRs during FJH process, multiple characterization techniques were employed to elucidate the underlying mechanisms. TG and DTG analyses under nitrogen atmosphere (Fig. 5**d** and **Fig. S5**) revealed three distinct stages: The initial weight loss (200–600 °C) was attributed to the volatilization of incompletely pyrolyzed siloxanes, followed by a stable stage (600–850 °C), with the third stage (850–1200 °C) corresponding to further carbon condensation and silicon oxide formation. At an SFR of 2.0, the ash exhibited negligible weight loss (9.3 %) at 850 °C compared to 26.1 % for SFR = 0.0. This trend continued at 1200 °C with 34.4 % versus 44.5 %. The DSC results (Fig. 5**e**) demonstrated that as the SFR increased from 0.0 to 3.0, the maximum heat flow during ash heating from room temperature to 1200 °C decreased from 29.1 mW/mg to 10.1 mW/mg, indicating reduced energy consumption required to reach the same targeted temperature.

The C1s core-level XPS spectra of the pyrolysis residue (**Fig. S6**) reveal that an increase in SFR alters the carbon element properties in the pyrolysis residue[52]. Specifically, the relative content of sp^2/sp^3 carbon increased from 8.42 % (SFR = 0.0) to 43.84 % (SFR = 2.0) (Fig. 5**f**), followed by a notable increase to 97.15 % at SFR of 3.0. Moreover, the FTIR spectra (**Fig. S7**) demonstrate that the concentration of silicon oxide increased with the SFR increasing, which suggested a corresponding decreased in the carbon content of the ashes.

These results collectively demonstrate that higher SFR not only enhances the yield and quality of syngas, but also modifies the physicochemical properties of the resulting residues, ultimately influencing the SiC formation during FJH process. As the SFR increased from 0 to 3, the reduced volatile content in the ashes led to a significant decrease in the energy consumption required to reheat the ash to the same temperature. This observation further confirmed that peak temperatures during FJH reached were achieved at an SFR of 2.0 (Fig. 5**c**). Furthermore, the residual carbon in the ash exhibited various forms, with aromatic carbon contents increasing as the SFR rose, which promotes SiC formation at elevated temperatures.

3.4. WEG performance of the SiC based materials

Joule heating-generated silicon carbide not only exhibits high hardness and heat resistance, but also exhibits excellent electrical properties due to its content of graphene. The incorporation of graphene layers introduces capillary channels for water molecules (**Fig. S8**), facilitating their diffusion through capillary action[53]. Furthermore, the inherent negative electrical properties of SiC[54], combined with the graphene surface, enable the formation of cation channels, thereby enhancing charge transport[55]. Consequently, the hybrid composition of SiC and graphene offers emerges as an ideal conductive material for water evaporation-induced electricity generators (WEGs)[56]. To fabricate this composite, SiC and graphene materials were synthesized by using a simple in situ dip coating and drying method[57] on PET nonwoven fabric substrate (Fig. 6**a**).

Fig. 6**b and 6c** illustrate the open circuit voltage (V_{OC}) and short circuit current (I_{SC}) characteristics of synthetic graphene-based WEGs (G-WEGs, dotted line) and SiC-graphene composite-based WEGs (SC-WEGs, solid line) under varying loaded material with different resistances. As the resistance decreases, both the V_{OC} decrease and the I_{SC} increase for both WEG types, with SC-WEGs exhibited better electrical response. The SC-WEG achieved a maximum V_{OC} of of 502 mV at ~ 16 kΩ, and a maxium I_{SC} of 9.80 μA at ~ 8 kΩ, representing a 21–39 %

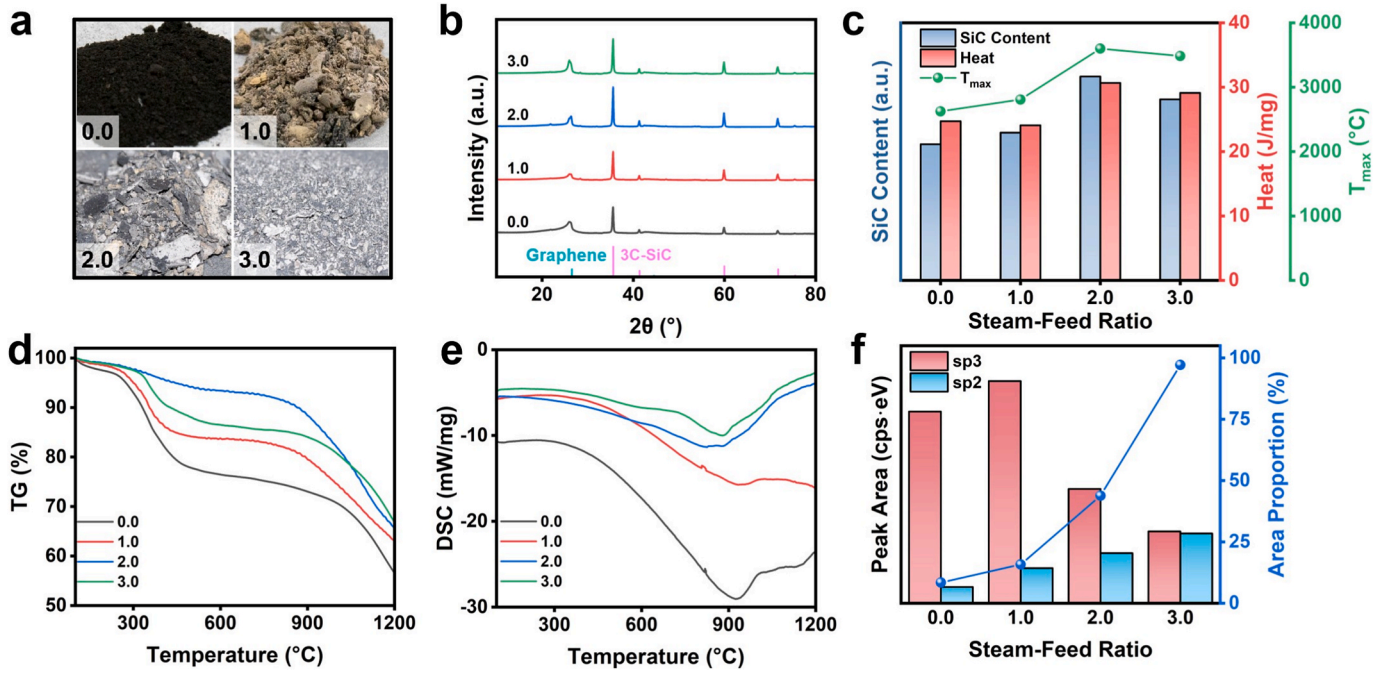

Fig. 5. Effect of steam-feed ratio on SiC synthesis. a, Optical photographs of the pyrolysis residues, **b,** Effect of SFR on the XRD spectra and **c,** corresponding SiC content intensity, heat released by capacitors discharge, and peak temperature. **d,** TG curves and **e,** DSC curves ranging from 100 °C to 1200 °C in nitrogen atmosphere. **f,** C–C sp3 and sp2 peak area and sp2 to sp3 relative area proportion of pyrolysis residues in C *1 s* core-level XPS spectra.

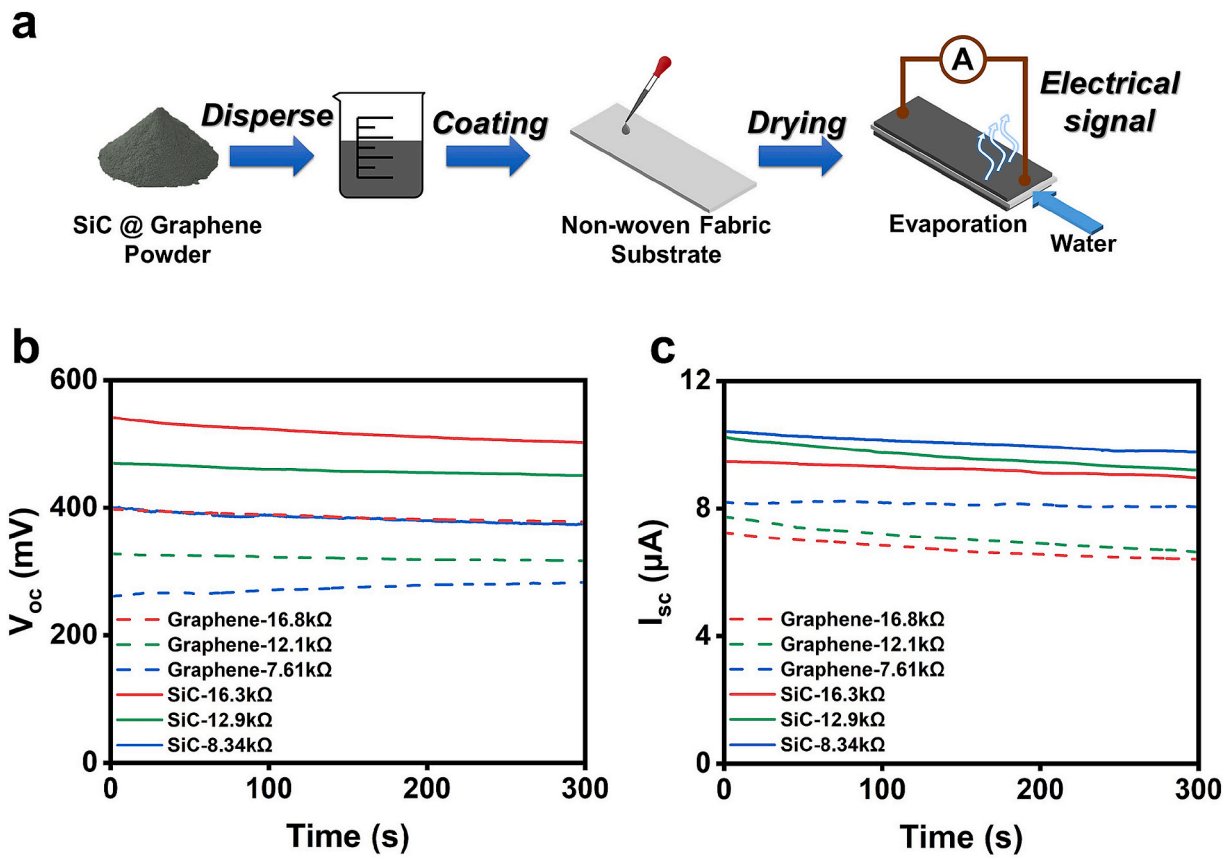

Fig. 6. Synthesis and performance of SiC based WEG. a, Preparation process of the water evaporation-induced electricity generators. **b,** Open circuit voltage and **c,** short circuit current of synthesized SiC and graphene materials at different approximate resistances of 16 kΩ, 12 kΩ and 8 kΩ.

improvement over G-WEGs. Compared to other similar WEGs (Fig. S9), the SiC-graphene composite material synthesized via FJH from pyrolysis residue provides an enhanced electrical signal output capability, highlighting its potential for sensor applications.

4. Conclusion

In summary, a two-step thermochemical process combining steam gasification and flash Joule heating (FJH) was developed to upcycle organic siloxane waste into H_2-enriched syngas and silicon carbide (SiC). By optimizing the steam-to-feed ratio (SFR) and reaction temperature, a carbon conversion rate of 75.9 % was achieved at 800 °C (SFR = 2), with a maximum syngas yield of 42.23 mmol/g observed at 900 °C. The pyrolysis residue was effectively transformed into a SiC-graphene composite using FJH method. The enhanced SiC formation efficiency at SFR = 2 indicates that effective siloxane gasification significantly facilitates the subsequent FJH process, likely due to the reduction in volatiles and increased aromatic carbon content in the pyrolysis residue. The resulting SiC based material demonstrated superior electricity generation during water evaporation compared to the flash graphene. This process achieves complete recycling of carbon and silicon from siloxane waste without generating by-products, offering a sustainable and scalable approach for siloxane waste management and upcycling, supporting circular economy initiatives.

CRediT authorship contribution statement

Huiyang Bi: Writing – original draft, Data curation, Methodology, Investigation, Validation. **Bo Wu:** Investigation, Validation. **Mingyue Yan:** Investigation, Validation. **Chen Sun:** Writing – review & editing, Investigation, Validation, Supervision, Conceptualization, Resources. **Zhongjian Li:** Resources. **Yang Hou:** Resources. **Lecheng Lei:** Conceptualization, Supervision. **Bin Yang:** Project administration, Writing – review & editing, Conceptualization, Resources.

Declaration of competing interest

The authors declare that they have no known competing financial interests or personal relationships that could have appeared to influence the work reported in this paper.

Acknowledgment

We are grateful for financial support from the “Lingyan” R&D Plan Project of Zhejiang Province (2023C03140).

Appendix A. Supplementary data

Supplementary data to this article can be found online at https://doi.org/10.1016/j.cej.2025.161706.

Data availability

Data will be made available on request.

References

[1] K. Kuciński, H. Stachowiak-Dłużyńska, G. Hreczycho, Catalytic silylation of o-nucleophiles via Si-H or Si-C bond cleavage: a route to silyl ethers, silanols and siloxanes, Coord. Chem. Rev. 459 (2022) 214456, https://doi.org/10.1016/j.ccr.2022.214456.
[2] C. Huang, B. Chattopadhyay, V. Gevorgyan, Silanol: a traceless directing group for Pd-catalyzedo-alkenylation of phenols, J. Am. Chem. Soc. 133 (2011) 12406–12409, https://doi.org/10.1021/ja204924j.

[3] J. Yu, Y. Liu, Cyclic polysiloxanes with linked cyclotetrasiloxane subunits, Angew. Chem. Int. Ed. 56 (2017) 8706–8710, https://doi.org/10.1002/anie.201703347.
[4] Q. Bu, E. Gońka, K. Kuciński, L. Ackermann, Cobalt-catalyzed hiyama-type C-H activation with arylsiloxanes: versatile access to highlyortho-decorated biaryls, Chemistry-a, European Journal. 25 (2019) 2213–2216, https://doi.org/10.1002/chem.201806114.
[5] Y. Wang, A. Attam, H. Fan, W. Zheng, W. Liu, Engineering of siloxanes for stabilizing silicon anode materials, Small 19 (2023), https://doi.org/10.1002/smll.202303804.
[6] J.Y. Domoradzki, C.M. Sushynski, J.M. Sushynski, D.A. McNett, C. Van Landingham, K.P. Plotzke, Metabolism and disposition of [14C]-methylcyclosiloxanes in rats, Toxicol. Lett. 279 (2017) 98–114, https://doi.org/10.1016/j.toxlet.2017.05.002.
[7] D. Krenczkowska, K. Mojsiewicz-Pieńkowska, B. Wielgomas, K. Cal, R. Bartoszewski, S. Bartoszewska, Z. Jankowski, The consequences of overcoming the human skin barrier by siloxanes (silicones) Part 1. Penetration and permeation depth study of cyclic methyl siloxanes, Chemosphere. 231 (2019) 607–623, https://doi.org/10.1016/j.chemosphere.2018.09.154.
[8] Y. Zhang, J. Li, H. Liu, Y. Ji, Z. Zhong, F. Su, Recent advances in rochow-müller process research: driving to molecular catalysis and to a more sustainable silicone industry, ChemCatChem 11 (2019) 2757–2779, https://doi.org/10.1002/cctc.201900385.
[9] S. Wang, J. Liu, S.V. Pisupati, D. Li, Z. Wang, J. Cheng, Dispersion mechanism of coal water slurry prepared by mixing various high-concentration organic waste liquids, Fuel 287 (2021) 119340, https://doi.org/10.1016/j.fuel.2020.119340.
[10] B. Dereli, B. Gürel, G. Karaca Dolgun, A. Keçebaş, Comprehensive study on incineration-based disposal of hazardous gas and liquid wastes from used lubricating oil refineries, Process Saf. Environ. Protect. 184 (2024) 79–95, https://doi.org/10.1016/j.psep.2024.01.077.
[11] M. Yan, H. Bi, H. Wang, C. Xu, L. Chen, L. Zhang, S. Chen, X. Xu, Q. Chen, Y. Jia, B. Wu, Z. Li, Y. Hou, L. Lei, B. Yang, Advanced soft-sensing techniques for predicting furnace temperature in industrial organic waste gasification, Process Saf. Environ. Protect. 190 (2024) 1253–1262, https://doi.org/10.1016/j.psep.2024.07.124.
[12] H. Bi, C. Deng, L. Chen, X. Zhao, Z. Li, Y. Hou, L. Lei, B. Yang, Numerical simulation study on the formation and control of hcl during the gasification of industrial organic hazardous waste, Process Saf. Environ. Protect. 175 (2023) 774–782, https://doi.org/10.1016/j.psep.2023.05.094.
[13] P. Beekman, A. Enciso-Martinez, S.P. Pujari, L.W.M.M. Terstappen, H. Zuilhof, S. Le Gac, C. Otto, Organosilicon uptake by biological membranes, Commun. Biol. 4 (2021), https://doi.org/10.1038/s42003-021-02155-5.
[14] F. Qi, G. Zhu, Y. Zhang, H. Li, S. Li, C. Yang, J. Zhang, Eco-friendly recycling of silicon-rich lye: synthesis of hierarchically structured calcium silicate hydrate and its application for phosphorus removal, Sci. Total Environ. 848 (2022) 157431, https://doi.org/10.1016/j.scitotenv.2022.157431.
[15] S. Sun, Y. Shi, J. Zhang, B. Wu, W. Xu, H. Cao, L. Wang, Analysis and pathway exploration of high-boiling residues for methyl-chlorosilane-monomers production, Chem. Eng. J. 483 (2024) 149201, https://doi.org/10.1016/j.cej.2024.149201.
[16] Z. Zhang, C. Chen, Z. Ao, L. Chen, N. Zhang, Alcl3-grafted mcm-41 as a new catalyst for the catalytic cleavage of the Si-Si bond of methylchlorodisilanes to methylchloromonosilanes, Phosphorus, Sulfur, and Silicon and the Related, Elements 185 (2010) 2355–2361, https://doi.org/10.1080/10426501003645860.
[17] J. Sousa Cardoso, V. Silva, D. Eusébio, I. Lima Azevedo, L.A.C. Tarelho, Techno-economic analysis of forest biomass blends gasification for small-scale power production facilities in the Azores, Fuel 279 (2020) 118552, https://doi.org/10.1016/j.fuel.2020.118552.
[18] M. Abou Rjeily, C. Gennequin, H. Pron, E. Abi-Aad, J.H. Randrianalisoa, Pyrolysis-catalytic upgrading of bio-oil and pyrolysis-catalytic steam reforming of biogas: a review, Environ. Chem. Lett. 19 (2021) 2825–2872, https://doi.org/10.1007/s10311-021-01190-2.
[19] M. Yan, T. Liang, H. Zhao, Y. Bi, T. Wang, T. Yu, Y. Zhang, Model properties and clinical application in the finite element analysis of knee joint: a review, Orthop. Surg. 16 (2024) 289–302. https://doi.org/10.1111/os.13980.
[20] C. Zhang, Y. Zhao, Z. Feng, L. Wang, Q. Meng, Y. Lu, Q. Gao, Comparative study on the chemical structure characteristics of lump coal during superheated water vapor pyrolysis and conventional pyrolysis, Energy 276 (2023) 127613, https://doi.org/10.1016/j.energy.2023.127613.
[21] S. Zhao, P. Yang, X. Liu, Q. Zhang, J. Hu, Synergistic effect of mixing wheat straw and lignite in co-pyrolysis and steam co-gasification, Bioresour. Technol. 302 (2020) 122876, https://doi.org/10.1016/j.biortech.2020.122876.
[22] A. Gurgul, W. Szczepaniak, M. Zabłocka-Malicka, Incineration and pyrolysis vs. steam gasification of electronic waste, Sci. Total Environ. 624 (2018) 1119–1124, https://doi.org/10.1016/j.scitotenv.2017.12.151.
[23] R. He, N. Zhou, K. Zhang, X. Zhang, L. Zhang, W. Wang, D. Fang, Progress and challenges towards additive manufacturing of sic ceramic, J. Adv. Ceram. 10 (2021) 637–674, https://doi.org/10.1007/s40145-021-0484-z.
[24] W. Zhang, A novel ceramic with low friction and wear toward tribological applications: boron carbide-silicon carbide, Adv. Colloid. Interface. Sci. 301 (2022) 102604, https://doi.org/10.1016/j.cis.2022.102604.
[25] G. Feng, S. Wang, S. Li, R. Ge, X. Feng, J. Zhang, Y. Song, X. Dong, J. Zhang, G. Zeng, Q. Zhang, G. Ma, Y.D. Chuang, X. Zhang, J. Guo, Y. Sun, W. Wei, W. Chen, Highly selective photoelectroreduction of carbon dioxide to ethanol over graphene/silicon carbide composites, Angew. Chem. Int. Ed. 62 (2023), https://doi.org/10.1002/anie.202218664.
[26] M. Mansouri, C. Díaz, F. Martín, Optoelectronic properties of electron-acceptor molecules adsorbed on graphene/silicon carbide interfaces, Commun. Mater. 5 (2024), https://doi.org/10.1038/s43246-024-00549-6.
[27] M. Widmann, M. Niethammer, D.Y. Fedyanin, I.A. Khramtsov, T. Rendler, I. D. Booker, J. Ul Hassan, N. Morioka, Y. Chen, I.G. Ivanov, N.T. Son, T. Ohshima, M. Bockstedte, A. Gali, C. Bonato, S. Lee, J. Wrachtrup, Electrical charge state manipulation of single silicon vacancies in a silicon carbide quantum optoelectronic device, Nano Lett. 19 (2019) 7173–7180, https://doi.org/10.1021/acs.nanolett.9b02774.
[28] Z. Zhu, C. Tu, B. Xiao, L. Long, F. Jiang, S. Liu, Research on characteristics of sic fet/si igbt and sic mosfet/si igbt hybrid switches, IEEE, 2022.
[29] G. Yuan, J.P. Forna-Kreutzer, P. Xu, S. Gonderman, C. Deck, L. Olson, E. Lahoda, R. O. Ritchie, D. Liu, In situ high-temperature 3d imaging of the damage evolution in a sic nuclear fuel cladding material, Mater. Des. 227 (2023) 111784. https://doi.org/10.1016/j.matdes.2023.111784.
[30] K.M. Wyss, D.X. Luong, J.M. Tour, Large-scale syntheses of 2d materials: flash joule heating and other methods, Adv. Mater. 34 (2022) 2106970, https://doi.org/10.1002/adma.202106970.
[31] X. He, P. Du, G. Yu, R. Wang, Y. Long, B. Deng, C. Yang, W. Zhao, Z. Zhang, K. Huang, M. Lei, X. Li, H. Wu, High-performance hydrogen evolution reaction catalytic electrodes by liquid joule-heating growth, Small Methods 7 (2023), https://doi.org/10.1002/smtd.202300544.
[32] W. Yang, L. Shang, X. Liu, S. Zhang, H. Li, Z. Yan, J. Chen, Ultrafast synthesis of nanocrystalline spinel oxides by joule-heating method, Chin. Chem. Lett. (2024) 109501, https://doi.org/10.1016/j.cclet.2024.109501.
[33] W. Chen, J. Chen, K.V. Bets, R.V. Salvatierra, K.M. Wyss, G. Gao, C.H. Choi, B. Deng, X. Wang, J.T. Li, C. Kittrell, N. La, L. Eddy, P. Scotland, Y. Cheng, S. Xu, B. Li, M.B. Tomson, Y. Han, B.I. Yakobson, J.M. Tour, Battery metal recycling by flash joule heating, Sci. Adv. 9 (2023) eadh5131, https://doi.org/10.1126/sciadv.adh5131.
[34] W. Zhu, H. Su, P. Bai, Z. Li, J. Zhang, J. Zhang, M. Li, Y. Chen, Y. Xu, A layered/spinel heterostructured cathode for li-ion batteries prepared by ultrafast joule heating, Chem. Eng. J. 480 (2024) 148045, https://doi.org/10.1016/j.cej.2023.148045.
[35] B. Deng, D.X. Luong, Z. Wang, C. Kittrell, E.A. McHugh, J.M. Tour, Urban mining by flash joule heating, Nat. Commun. 12 (2021), https://doi.org/10.1038/s41467-021-26038-9.
[36] Y. Cheng, J. Chen, B. Deng, W. Chen, K.J. Silva, L. Eddy, G. Wu, Y. Chen, B. Li, C. Kittrell, S. Xu, T. Si, A.A. Martí, B.I. Yakobson, Y. Zhao, J.M. Tour, Flash upcycling of waste glass fibre-reinforced plastics to silicon carbide, Nat. Sustain. (2024), https://doi.org/10.1038/s41893-024-01287-w.
[37] M.P. Kroonblawd, N. Goldman, J.P. Lewicki, Anisotropic hydrolysis susceptibility in deformed polydimethylsiloxanes, J. Phys. Chem. B 123 (2019) 7926–7935, https://doi.org/10.1021/acs.jpcb.9b07159.
[38] B.F. Guo, Y.J. Wang, Z.H. Qu, F. Yang, Y.Q. Qin, Y. Li, G.D. Zhang, J.F. Gao, Y. Shi, P. Song, L.C. Tang, Hydrosilylation adducts to produce wide-temperature flexible polysiloxane aerogel under ambient temperature and pressure drying, Small 20 (2024), https://doi.org/10.1002/smll.202309272.
[39] A.A. Kalinina, I.V. Elmanovich, M.N. Temnikov, M.A. Pigaleva, A.S. Zhiltsov, M. O. Gallyamov, A.M. Muzafarov, Hydrolytic polycondensation of diethoxydimethylsilane in carbonic acid, Rsc Adv. 5 (2015) 5664–5666, https://doi.org/10.1039/C4RA13619E.
[40] Y. Xu, X. Sun, D. Wu, Y. Sun, Y. Yang, H. Yuan, F. Deng, Z. Wu, Ammonia catalyzed hydrolysis-condensation kinetics of tetraethoxysilane/dimethyldiethoxysilane mixtures studied by 29si nmr and saxs, J. Solut. Chem. 36 (2007) 327–344, https://doi.org/10.1007/s10953-006-9117-y.
[41] J. Kiecherer, C. Bänsch, T. Bentz, M. Olzmann, Pyrolysis of ethanol: a shock-tube/tof-ms and modeling study, Proc. Combust. Inst. 35 (2015) 465–472, https://doi.org/10.1016/j.proci.2014.05.086.
[42] H. Hashemi, J.M. Christensen, P. Glarborg, High-pressure pyrolysis and oxidation of ethanol, Fuel 218 (2018) 247–257, https://doi.org/10.1016/j.fuel.2017.12.085.
[43] B. Xu, Y. Wang, G. Liu, Reactive molecular dynamics study on catalytic pyrolysis and steam reforming of hydrocarbon fuel, J. Anal. Appl. Pyrolysis. 169 (2023) 105875, https://doi.org/10.1016/j.jaap.2023.105875.
[44] J. Ju, K. You, S. Liu, Y. She, C. Zou, Effect of water vapor on pore structure, surface functional groups, and combustion performance of pyrolytic semicoke, ACS Omega 7 (2022) 24587–24595, https://doi.org/10.1021/acsomega.2c02396.
[45] Y.J. Cho, K. Lu, Water vapor oxidation of sic layer in surrogate triso fuel particles, Compos. B Eng. 215 (2021) 108807, https://doi.org/10.1016/j.compositesb:2021.108807.
[46] C. Arnal, M.U. Alzueta, A. Millera, R. Bilbao, Influence of water vapor addition on soot oxidation at high temperature, Energy 43 (2012) 55–63, https://doi.org/10.1016/j.energy.2012.03.036.
[47] K. Koumoto, S. Takeda, C.H. Pai, T. Sato, H. Yanagida, High-resolution electron microscopy observations of stacking faults in β-sic, J. Am. Ceram. Soc. 72 (1989) 1985–1987. https://doi.org/10.1111/j.1151-2916.1989.tb06014.x.
[48] K.R. Carduner, S.S. Shinozaki, M.J. Rokosz, C.R. Peters, T.J. Whalen, Characterization of β-silicon carbide by silicon-29 solid-state nmr, transmission electron microscopy, and powder x-ray diffraction, J. Am. Ceram. Soc. 73 (1990) 2281–2286. https://doi.org/10.1111/j.1151-2916.1990.tb07589.x.
[49] Z. Cheng, J. Liang, K. Kawamura, H. Zhou, H. Asamura, H. Uratani, J. Tiwari, S. Graham, Y. Ohno, Y. Nagai, T. Feng, N. Shigekawa, D.G. Cahill, High thermal conductivity in wafer-scale cubic silicon carbide crystals, Nat. Commun. 13 (2022) 7201, https://doi.org/10.1038/s41467-022-34943-w.

[50] S.V. Didziulis, P.D. Fleischauer, Effects of chemical treatments on sic surface composition and subsequent mos2 film growth, Langmuir 6 (1990) 621–627, https://doi.org/10.1021/la00093a017.
[51] L. Silva, J.L.E. Campos, T.F.D. Fernandes, J.N. Rocha, L.R.P. Machado, E.M. Soares, D.R. Miquita, H. Miranda, C. Rabelo, O.P. Vilela Neto, A. Jorio, L.G. Cançado, Raman spectroscopy analysis of number of layers in mass-produced graphene flakes, Carbon 161 (2020) 181–189, https://doi.org/10.1016/j.carbon.2020.01.050.
[52] A. Shchukarev, D. Korolkov, Xps study of group ia carbonates, Open Chem. 2 (2004) 347–362, https://doi.org/10.2478/BF02475578.
[53] X. Zhang, Y. Wang, X. Zhang, C. Lou, J. Lin, T. Li, Preparation and study of bark-like mxene based high output power hydroelectric generator, Chem. Eng. J. 465 (2023) 142582, https://doi.org/10.1016/j.cej.2023.142582.
[54] R. Gong, H. Song, J. Yang, H. Liu, Optimization of sic cleaning process based on zeta potential, Academic, J. Sci. Technol. 5 (2023) 158–162. https://doi.org/10.54097/ajst.v5i2.6855.
[55] J. Zhang, P. Cui, J. Wang, H. Meng, Y. Ge, C. Feng, H. Liu, Y. Meng, Z. Zhou, N. Xuan, B. Zhang, G. Cheng, Z. Du, Paper-based hydroelectric generators for water evaporation-induced electricity generation, Adv. Sci. 10 (2023), https://doi.org/10.1002/advs.202304482.
[56] Y. Han, D. Pang, Z. Xiong, X. Zhao, C. Li, X. Pang, J. Sun, Flexible silicon carbide based nano-generator driven by water evaporation, Chem. Phys. 538 (2020) 110858, https://doi.org/10.1016/j.chemphys.2020.110858.
[57] S. Xu, Y. Zhao, S. Jiao, Z. Wang, Z. Yu, C. Sun, X. Liu, Microalgae film-derived water evaporation-induced electricity generator with negative carbon emission, Adv. Sci. 11 (2024), https://doi.org/10.1002/advs.202400856.